HYDRAULIC RAM PRESSURE MEASUREMENTS

Clifford Milton Holm

NAVAL POSTGRADUATE SCHOOL
Monterey, California

THESIS

HYDRAULIC RAM PRESSURE MEASUREMENTS

by

Clifford Milton Holm

December 1974

Thesis Advisor: H.L. Power, Jr.

UNCLASSIFIED

SECURITY CLASSIFICATION OF THIS PAGE (When Data Entered)

REPORT DOCUMENTATION PAGE		READ INSTRUCTIONS BEFORE COMPLETING FORM
1. REPORT NUMBER	2. GOVT ACCESSION NO.	3. RECIPIENT'S CATALOG NUMBER
4. TITLE (and Subtitle) Hydraulic Ram Pressure Measurements		5. TYPE OF REPORT & PERIOD COVERED Master's Thesis; December 1974 6. PERFORMING ORG. REPORT NUMBER
7. AUTHOR(s) Clifford Milton Holm		8. CONTRACT OR GRANT NUMBER(s)
9. PERFORMING ORGANIZATION NAME AND ADDRESS Naval Postgraduate School Monterey, California 93940		10. PROGRAM ELEMENT, PROJECT, TASK AREA & WORK UNIT NUMBERS
11. CONTROLLING OFFICE NAME AND ADDRESS Naval Postgraduate School Monterey, California 93940		12. REPORT DATE December 1974 13. NUMBER OF PAGES 51
14. MONITORING AGENCY NAME & ADDRESS(if different from Controlling Office) Naval Postgraduate School Monterey, California 93940		15. SECURITY CLASS. (of this report) Unclassified 15a. DECLASSIFICATION/DOWNGRADING SCHEDULE

16. DISTRIBUTION STATEMENT (of this Report)

Approved for public release; distribution unlimited.

17. DISTRIBUTION STATEMENT (of the abstract entered in Block 20, if different from Report)

18. SUPPLEMENTARY NOTES

19. KEY WORDS (Continue on reverse side if necessary and identify by block number)

Hydraulic Ram Pressure

20. ABSTRACT (Continue on reverse side if necessary and identify by block number)

Hydraulic ram concerns the dynamic loads and catastrophic failure of liquid-filled fuel tanks impacted by high speed projectiles. Hydraulic ram is divided into two phases: the shock phase and the drag phase. Analytic models have been proposed for the shock phase by Yurkovich and for the drag phase by Lundstrom. An attempt was made to correlate these theoretical pressure predictions with experimental data

DD FORM 1 JAN 73 1473 EDITION OF 1 NOV 65 IS OBSOLETE
S/N 0102-014-6601 |
(Page 1)

UNCLASSIFIED
SECURITY CLASSIFICATION OF THIS PAGE (When Data Entered)

(20. ABSTRACT Continued)

obtained from 0.222 caliber projectiles impacting a small water-filled tank. This comparison showed reasonable correlation but indicates that more work must be done to permit predictions of hydraulic ram pressures accurate enough for the purpose of fuel cell design.

Hydraulic Ram Pressure Measurements

by

Clifford Milton Holm
Lieutenant, United States Navy
B.S.M.E., University of Denver, 1965

Submitted in partial fulfillment of the
requirements for the degree of

MASTER OF SCIENCE IN AERONAUTICAL ENGINEERING

from the

NAVAL POSTGRADUATE SCHOOL
December 1974

ABSTRACT

Hydraulic ram concerns the dynamic loads and catastrophic failure of liquid-filled fuel tanks impacted by high speed projectiles. Hydraulic ram is divided into two phases: the shock phase and the drag phase. Analytic models have been proposed for the shock phase by Yurkovich and for the drag phase by Lundstrom. An attempt was made to correlate these theoretical pressure predictions with experimental data obtained from 0.222 caliber projectiles impacting a small water-filled tank. This comparison showed reasonable correlation but indicates that more work must be done to permit predictions of hydraulic ram pressures accurate enough for the purpose of fuel cell design.

TABLE OF CONTENTS

LIST OF FIGURES

LIST OF SYMBOLS

A	Cross sectional area of the deformed projectile
B	Velocity decay factor
C_D	Drag coefficient
D	Drag acting on projectile
E_o	Impact kinetic energy of the projectile
V	Projectile velocity
V_o	Projectile impact velocity
f	Equivalent flat plate area
m	Mass of projectile
t	Time
x	Projectile distance traveled in tank
ρ	Density of the fluid

I. INTRODUCTION

In recent years the problem of aircraft survivability has become increasingly important. The relative vulnerability of today's complex and costly aircraft to small-arms projectile impact combined with high procurement costs and shrinking defense budgets has emphasized the importance of survivability analysis during the preliminary design phase of air weapons development. If present combat aircraft are to be able to satisfy mission requirements and be cost effective, their vulnerability to the threat posed by warhead fragments or projectile impact must also be reduced.

Ballistic impact is a major factor in generating catastrophic failure of aircraft components, and aircraft fuel cells are the component most susceptible to this kind of damage. They have the largest surface area and volume of any of the vulnerable aircraft components. If a fuel cell is impacted by a projectile or fragment, the aircraft may be lost through fuel starvation, fire or explosion. Additionally the pressure created by a ballistic impact can damage the structure, or critical components such as pumps and valves within the cell, or indirectly damage components adjacent to it. To prevent or reduce damage of this nature the failure mechanisms of fuel cells must be understood.

Projectiles which penetrate fluid filled cells cause much more severe damage than that incurred by impact with

an empty cell. A projectile impacting a fluid filled cell creates pressure waves in the tank fluid that can cause catastrophic failure of the cell's structural components. The interaction of the fluid filled cell with the projectile is called hydraulic ram. This phenomenon is usually described by two primary phases: the shock phase and the drag phase.

The shock phase is created by the initial projectile impact wherein energy is transferred to the fluid, creating a strong hemispherical shock centered at the point of impact. As this shock moves radially from the point of impact a transient pressure pulse is created which can cause failure of the entry wall if it is sufficiently thin, or if it is cracked by the projectile penetration dynamics.

As the projectile moves on through the fluid a cavity is formed by flow separation from the projectile surface. This phase of hydraulic ram is named after the primary energy dissipation mechanism present and is called the drag phase [Ref. 1]. As the cavity continues to grow within the fluid, a pressure pulse is created which can cause damage throughout the fuel cell. Later, oscillation of the cavity volume produces another pressure pulse that pumps fuel from any damaged areas of the cell and may be sufficiently intense to cause additional failure of fuel cell components. The intensity of the drag phase pressure pulse is weaker than the shock phase pressure pulse but the

duration is much larger [Ref. 2]. Ultimate failure of the tank other than at the entry wall has generally been attributed to the drag phase.

Until recently little analytical work has been accomplished to understand the well documented effects of hydraulic ram on aircraft. Much of the theory is still in its infancy and the complete mechanism is complex, requiring detailed analytical and experimental efforts if correlation of theory and experiment is to be accomplished.

Research at the Naval Postgraduate School has been designed to isolate and observe the individual components of hydraulic ram. In the past, the Naval Postgraduate School ballistic range has been used to study the energy losses due to projectile penetration through the entry wall and during the drag phase. Measurements of the shock propagation through the fluid have also been undertaken. This study was designed to investigate the correlation of experimentally obtained pressure data with available analytical pressure prediction models.

II. BACKGROUND

It has been established that the loading and deformation of fuel cell walls or structural components is caused by a number of separate events which are known collectively as hydraulic ram. These events are conveniently separated into two phases: the shock phase occurs when a projectile first enters the fluid, and the drag phase takes place as the bullet traverses the tank.

The shock phase of hydraulic ram is created when the projectile enters the fluid filled tank and displaces fluid, thereby compressing it to very high pressures near the impact point. This localized high pressure creates a shock wave which moves radially outward into the fluid. Due to geometric expansion of the shock front the peak pressure is rapidly attenuated. The shock phase is characterized by very high local pressures, short durations (on the order of micro-seconds) and independence of tank geometry [Ref. 3]. Work by Stepka [Ref. 4] indicates that the shock strength is primarily dependent on the initial energy of the projectile and shows little sensitivity to the projectile shape or materials.

The drag phase is the second major component of hydraulic ram. As the projectile moves on through the fluid a pressure field is produced which acts to displace the fluid from the projectile path. This pressure field is the source of drag

that decelerates the projectile. The kinetic energy of the projectile is transferred to the fluid in the form of outward fluid motion. Unlike the shock phase, the fluid is accelerated gradually rather than impulsively and the peak pressure is much lower. The duration of the pressure pulse, however, is much longer and is generally credited with doing the majority of damage to a fuel cell. An important characteristic of the drag phase is the formation of a cavity behind the projectile. As the projectile moves through the tank and displaces the fluid it imparts a large radial velocity to the fluid and as a result, the fluid moves away from the projectile surface creating a cavity. This cavity is filled with liquid vapor and air that entered during projectile penetration of the tank entry wall. The outward motion of the cavity in the fluid is opposed by the restraining effect of the fuel cell walls. Eventually the existing fluid pressure and wall effects will halt cavity growth and cause a collapse. As the cavity collapses, it compresses to a high pressure the air and fluid vapors it contains. This leads, in turn, to a re-expansion of the cavity. Expansion and collapse repeat several times before all the stored energy is dissipated.

A. SHOCK FRONT PRESSURES

It has been found that the protrusion of a projectile into a tank fluid produces a hemispherical shock centered at

the point of impact [Ref. 5]. Projectile momentum and path after entry have no effect on the shock wave shape as it traverses the fluid. From these results it can be concluded that shock phase pressure characteristics may be predicted by assuming that the shock is the result of a point energy source release [Ref. 6].

To predict fuel cell pressures created by the shock phase, a program was developed at the U.S. Naval Postgraduate School [Ref. 6] based on the theory of Yurkovich [Ref. 2]. The theory assumes that the fuel cell walls are rigid and that the shock radius is proportional to a constant, power of time. Studies by Kappel [Ref. 7] show this power to be 0.9 for an ogive shaped projectile as used in this study.

To obtain the shock front jump conditions the one-dimensional Rankine-Hugoniot equations were coupled with the Tait equation of state for isothermal, compressible liquids. The changes in fluid properties across the shock front were assumed to be adiabatic and were calculated as a function of Mach number.

Conditions behind the shock were determined by assuming that the density profile behind the shock was given by a power law function of the radius and that the shock radius-time relationship was proportional to the 0.9 power of time.

Assuming a hemispherical shock wave propagating from the entry point of the projectile, the velocity profile was obtained using the continuity equation. The density and velocity distributions were then combined with the momentum equation to calculate the pressure profile.

From the total energy released in the shock phase, the shock Mach number as a function of shock radius was determined by assuming conservation of energy and calculating the resulting energy distribution behind the shock wave. With the shock Mach number and shock radius relationship determined the shock radius was calculated as function of time. From this information the shock Mach number and pressure distribution were determined as a function of time.

Although the Yurkovich model provides a method of predicting shock pressures, it provides no information as to the energy released by the projectile in the shock phase and is dependent upon the correct value being supplied for accurate results. An analytic expression for this energy as a function of wall, fluid and projectile characteristics is not available.

B. DRAG PHASE PRESSURES

The drag phase pressure field is generated by the projectile during the penetration of the bulk of the fluid. Lundstrom [Ref. 1] has analyzed this phase and a computer progarm based on this analysis has been developed by the Naval Weapons Center in an effort to facilitate the prediction of fuel cell pressures. Lundstrom's model assumes that a bullet will transition from a stable non-yawed attitude to a fully tumbled condition as it traverses the tank. The model may also be used for cases that include projectile breakup or projectiles that are tumbled on impact.

To obtain the pressure field created in the drag phase, Newton's Second Law and a simple expression for projectile drag was used to calculate the kinetic energy loss, path time history, and velocity of the projectile in the tumbled and untumbled states. Projectile parameters between the untumbled and fully tumbled conditions are obtained from a computer numerical integration code.

The effects of the bullet and cavity on the fluid were approximated by a distribution of sources along the bullet path. The potential due to these sources was expressed as an integral function of the source strength, its location and the distance to the point at which the pressure was calculated. From a model based on the conservation of energy, the source strength was calculated in terms of the cavity radius. Wall restraining effects on cavity growth were neglected so that the source strength approximation is increasingly inexact as the cavity radius approaches its maximum. The source strength was combined with the potential equation to obtain the change in potential with time. The desired drag phase pressures were obtained by substituting the time varying potential and fluid velocity into Bernoulli's Equation.

Based on work by Cole [Ref. 8] the effects of the reflected pressure waves due to the fuel cell walls were accounted for by considering the walls to be free surfaces. Reflected pressures were considered to result from a mirror image of the line of sources creating the incident pressure.

This method will not give correct fuel cell wall loadings because the assumption that the wall is a free surface results in a boundary condition of zero pressure perturbation at the wall. The model also does not include reflected waves from the cavity surface, and solutions given by it are not valid when sufficient time has elapsed for this to occur. Reasonable results, however, can be expected if the point of interest is located away from the wall surface, for times below those required for waves to reflect from the cavity surface.

III. DESCRIPTION OF BALLISTIC RANGE COMPONENTS AND PROCEDURE

The basic elements of the ballistic range used for the study are shown in Figure III-1. The down range view of the ballistic range in Figure III-2 depicts the chronograph screen arrangement and the test tank.

A .222 caliber Remington rifle was used to obtain 7,493 in-lb and 12,323 in-lb impact energy levels tested. Figures III-3 and III-4 display the shapes and parameters of the projectiles used.

Avtron No. A914T333 chronograph screens were used to provide start and stop pulses to the two Monsanto 101B counters. Bullet impact velocities were calculated using the known distance between screens and the bullet flight times obtained from the counters. The two readings were averaged to obtain the bullet velocity. To obtain the pressure trace, screen four, placed 1.5 inches in front of the tank, was used to initiate the oscilloscope single sweep circuit.

The tank used to simulate a fuel cell is shown in Figures III-5 and III-6. Its inner dimensions were 17.0 inches depth, 17.5 inches in width and 17.0 inches in height. It was constructed from 1-inch thick plexiglass held in position by a cubical tank frame formed by welding .25-inch thick by three-inch wide aluminum angle sections. The entry wall of the tank was fabricated from .5-inch thick mild steel plate

to simulate the rigid entry wall required in the Yurkovich analysis. Bullet entry into the tank with minimum loss of energy was accomplished by providing a 1-inch entry hole in the center of the front wall. The back wall was a .160-inch 7075-T6 aluminum plate. Both front and back walls were bolted to the basic aluminum frame.

Initially the tank was mounted on top of the metal stand shown in Figure III-5, but the force of bullet impact often lifted the tank clear of the rectangular supports into which it had been placed, and upset it. To prevent this, the tank was secured to the stand and the stand was restrained with 150 lbs of sandbags, and by supports bolted to the floor, in an effort to prevent it from sliding along the floor.

Figure III-7 shows the pressure transducer assembly. A Kistler 603H quartz pressure transducer was used. The transducer was threaded into a nylon ring which was in turn threaded into the end of a hollow 1-inch outside diameter stainless steel tube. This provided protection for the transducer from the water environment. The upper end of the tube was sealed with RTV for additional waterproofing. A tube with a 45° angle at the tip was used to obtain the pressure measurements along a radius from the impact point. The probe was held in position by an adjustable tank mount attached to the top of the tank, as in Figure III-5. Pressure levels were measured along a line 50° from the vertical, at varying radii from the point of bullet entry. Pressure measurements were taken from a minimum distance of 2 inches

outward to 8 inches at both energy levels. Physical intrusion of the probe housing into the bullet flight path precluded measurement at closer distances.

The probe output signal created by the passing pressure front was conditioned by a Kistler Model 504E charge amplifier equipped with a 545A14 filter and displayed on an oscilloscope. The single sweep oscilloscope trace was recorded by a Polaroid oscilloscope camera. Several shots at a given radius were made to insure data accuracy and consistency for each of the two impact energies tested.

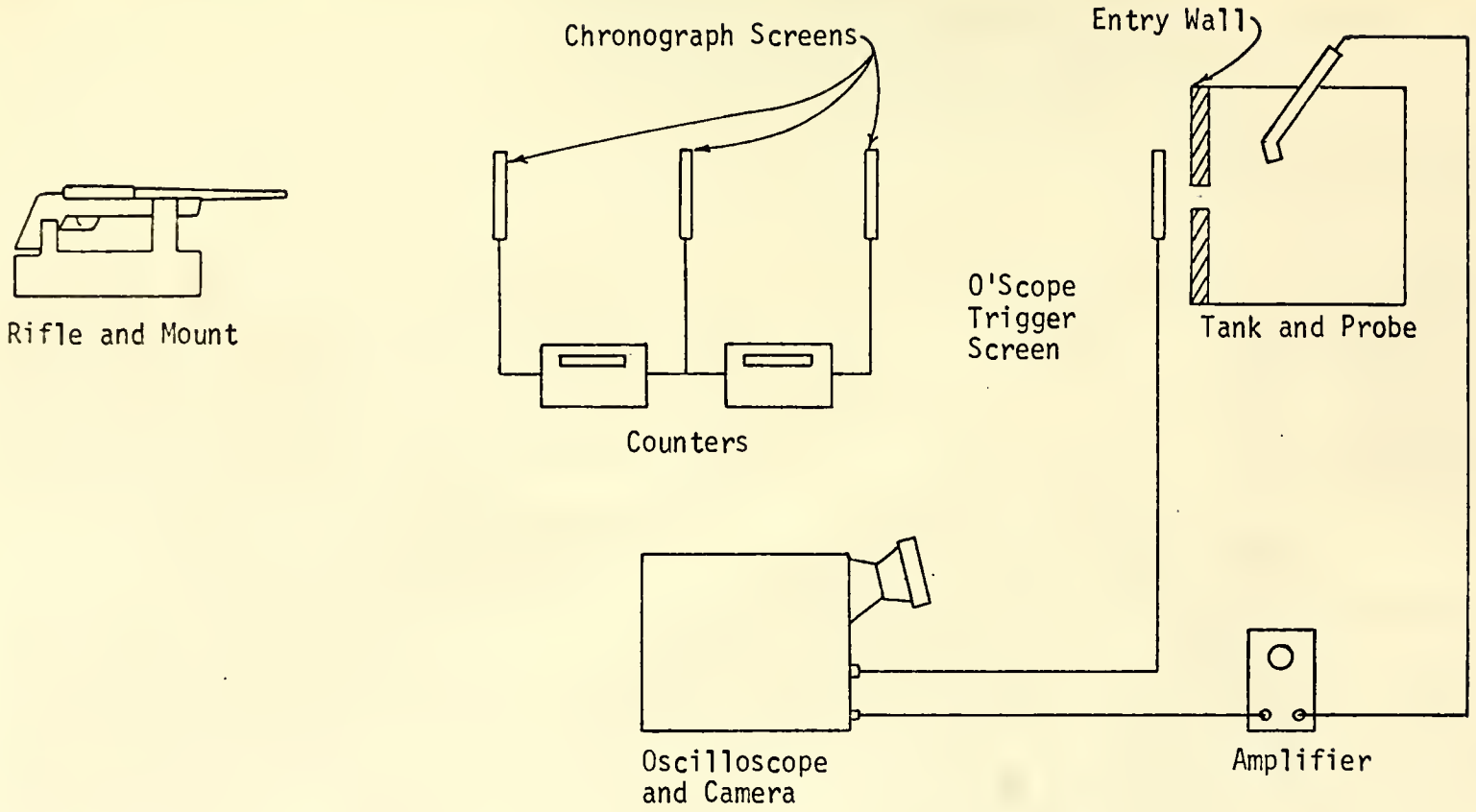

Figure III-1. Ballistic Range Components

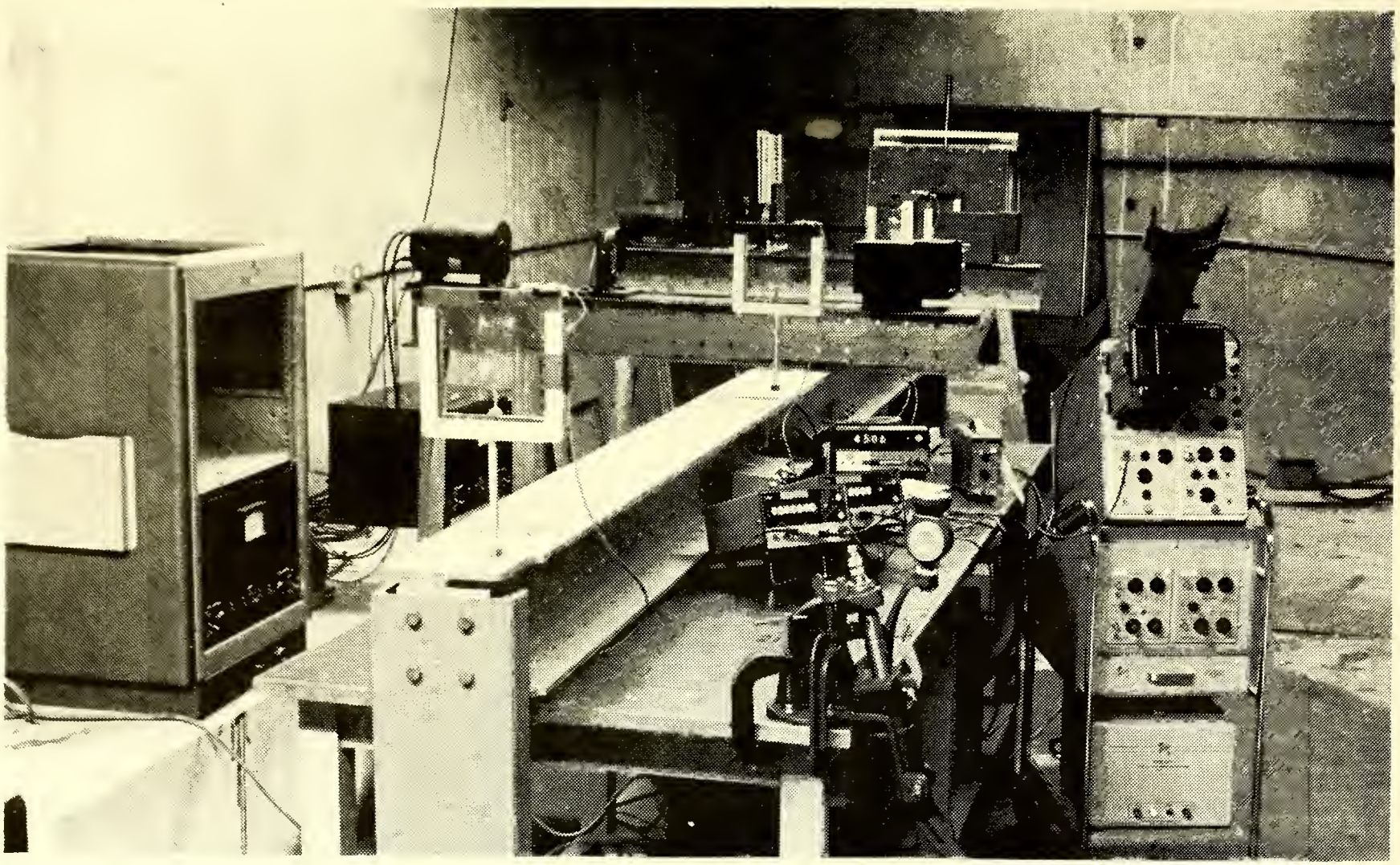

Figure III-2. Ballistic Range Configuration - (Down Range View)

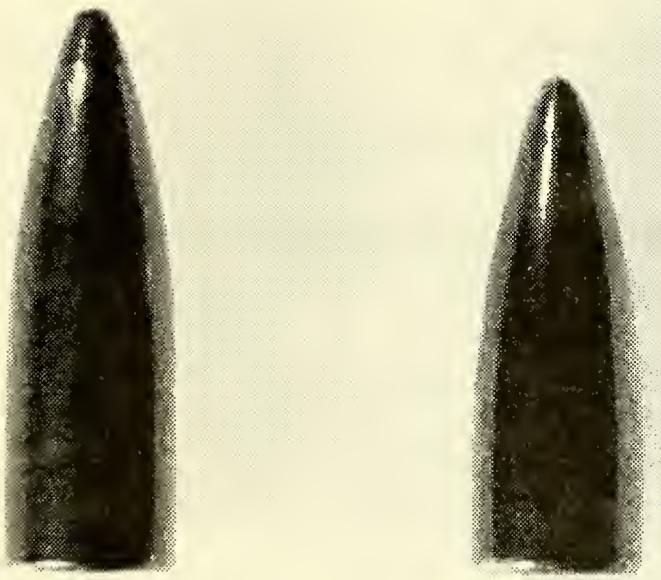

Figure III-3. Projectile Shapes
(Left: .222 caliber, $m = 7.85 \times 10^{-3}$ lb)
(Right: .222 caliber, $m = 6.43 \times 10^{-3}$ lb)

caliber	.222 Remington	.222 Remington
Impact Velocity, V_o (ft/sec)	2500	2900
Projectile Mass, m (lbm)	6.43×10^{-3}	7.85×10^{-3}
Impact Energy, E_o (in-lb)	7493	12,323
Equivalent Flat Plate Area, $f = C_D A$ (in^2)	.044	.083

FIGURE III-4. Projectile Parameters

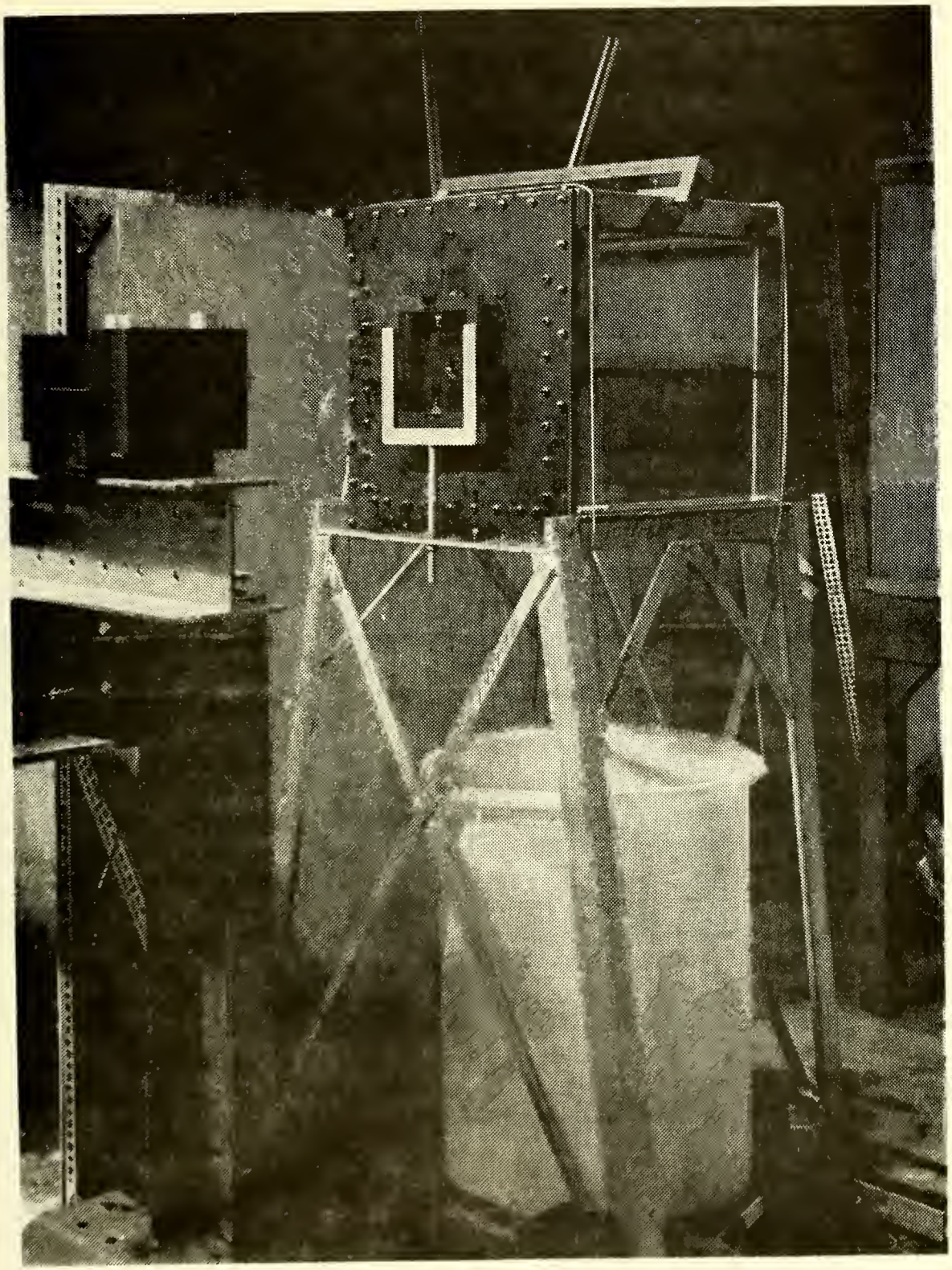

Figure III-5. Pressure Probe, Fuel Cell and Stand Installation

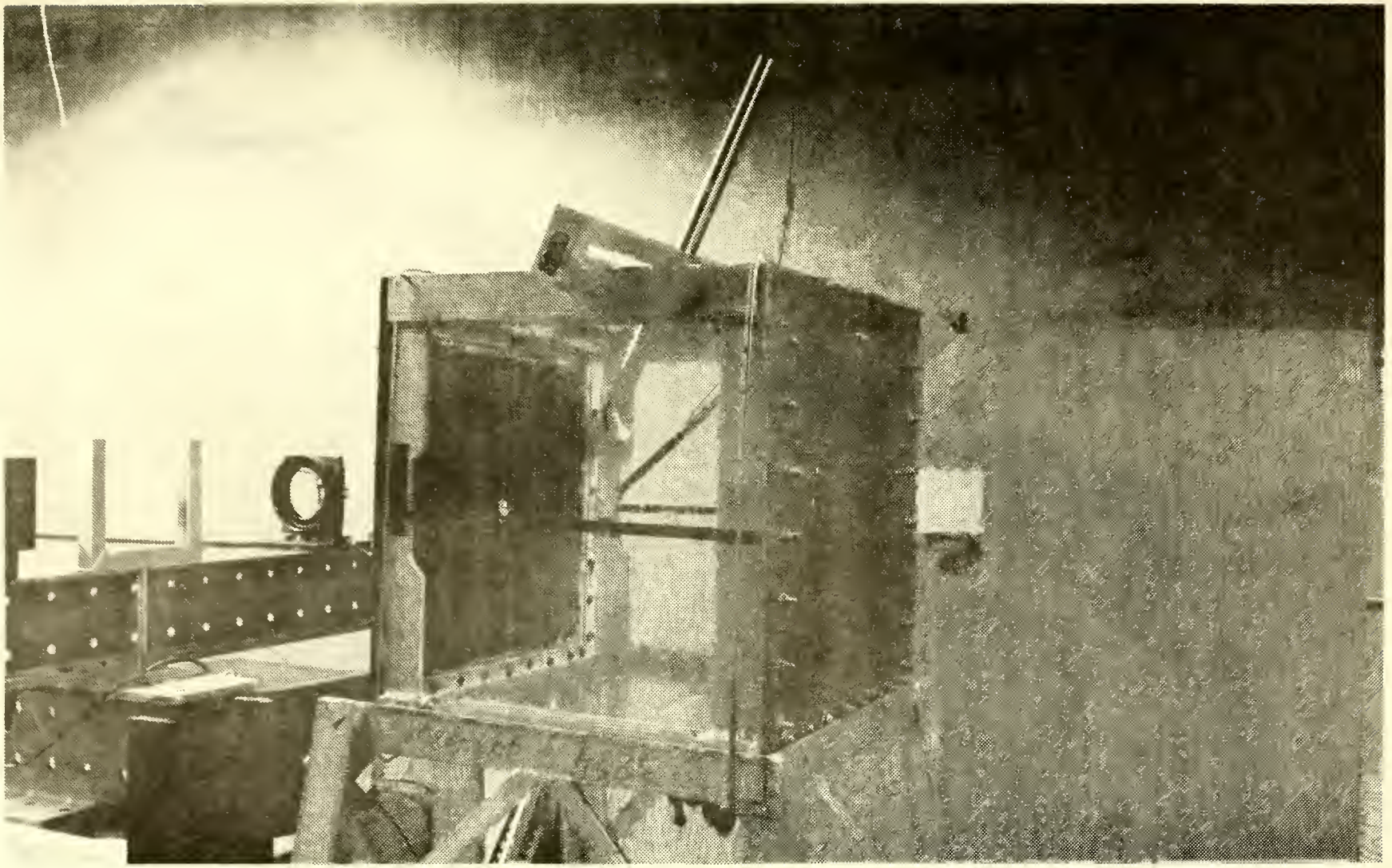

Figure III-6. Fuel Cell and Probe Installation

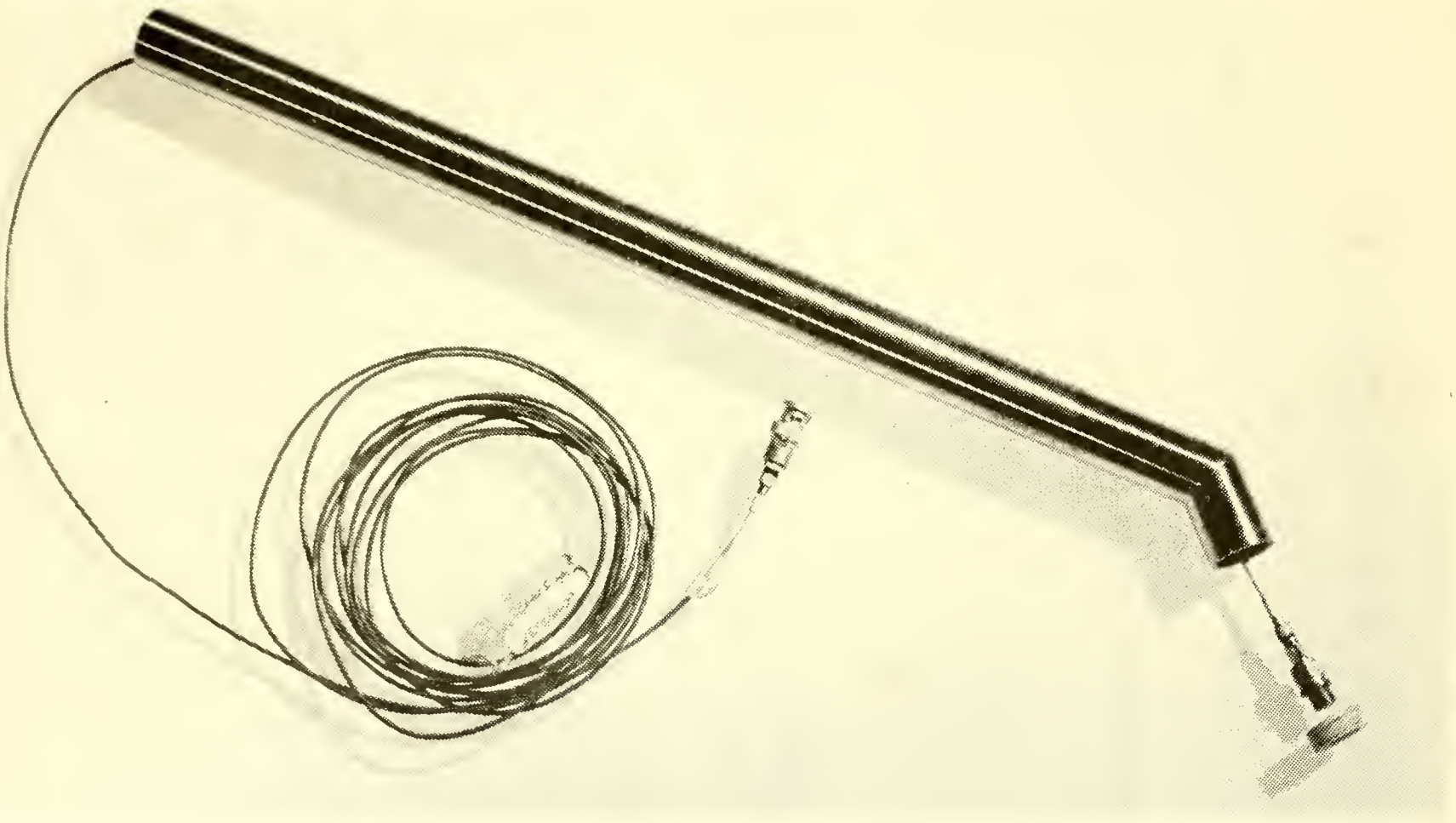

Figure III-7. Disassembled Probe and Housing

IV. DISCUSSION OF RESULTS

This research was conducted in an effort to verify two theoretical predictions of pressures caused by the hydraulic ram phenomena.

Typical experimental pressure traces obtained at varying radii for two projectile energy levels are shown in Figures IV-1 through IV-8. The 7,493 in-lb and 12,323 in-lb energy levels tested represent the highest and lowest energy levels to which the rifle cartridges could be loaded. Peak pressures obtained in the experimental curves decayed quite rapidly as distance from the impact point increased. The curves obtained closest to the entry point resembled a strong pressure disturbance with the peak pressure occurring at the leading edge of the pressure curve. As the distance from impact point increased, the disturbance assumed a more symmetrical shape. This was true for both energy levels. Pulse durations of over 200 microseconds were measured for the 12,393 in-lb energy level at a distance of two inches from the impact point. Pulse length decreased to approximately 100 microseconds at the eight-inch distance. Similar pulse durations, somewhat reduced in scale, were observed for the 7493 in-lb energy level.

Calculated shock phase pressures have durations of only a few microseconds and are a function of the energy dissipated by the projectile in the initial impact. Near the impact

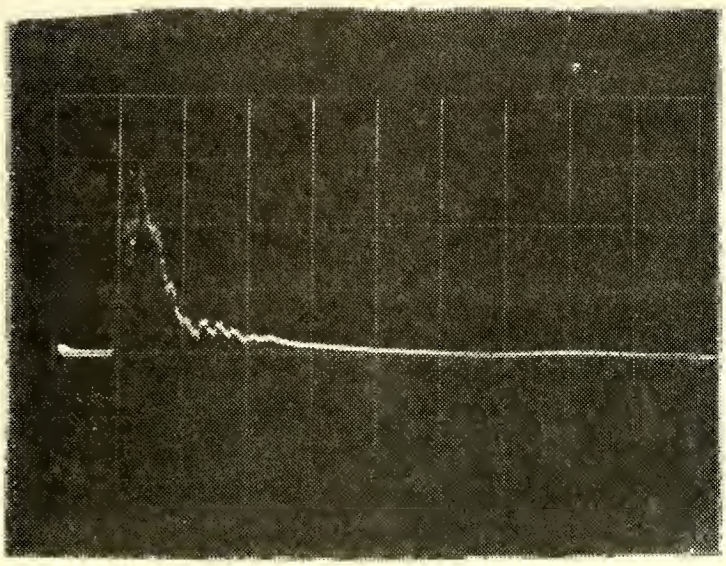

Radius = 2 in

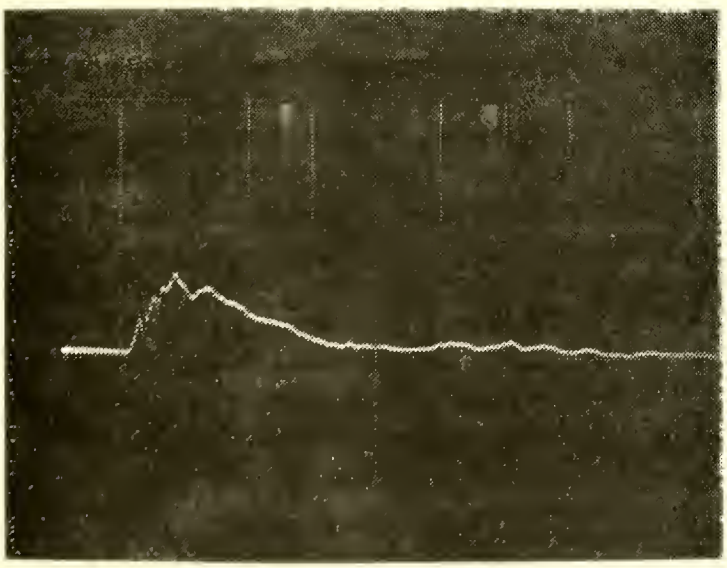

Radius = 3 in

Figure IV-1. Pressure vs. Time, E_o = 7,493 in-lb
Scale: 1250 lb/cm, 50 μsec/cm

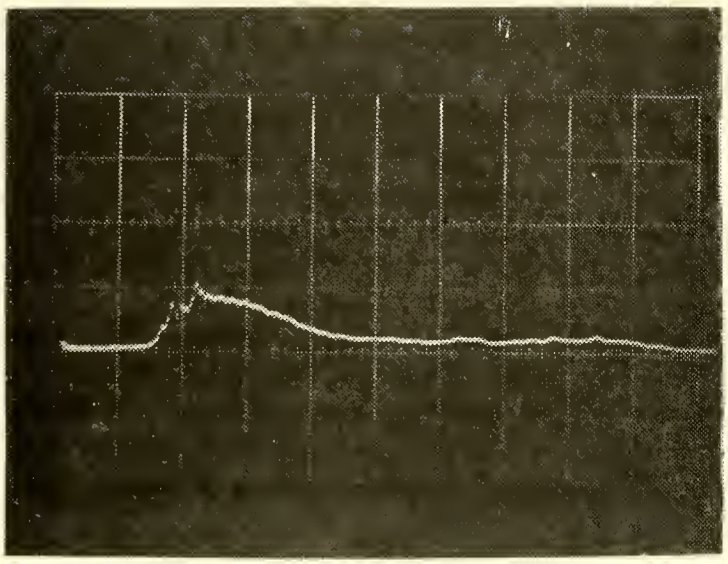

Radius = 4 in

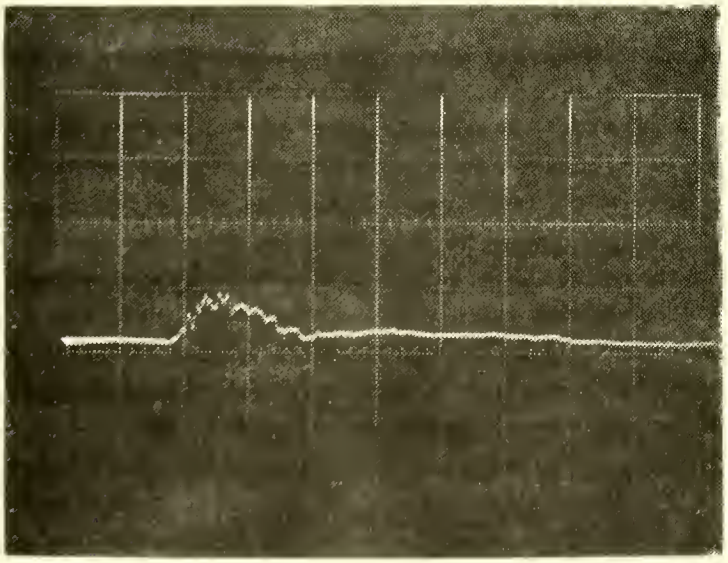

Radius = 5 in

FIGURE IV-2. Pressure vs. Time, E_o = 7,493 in-lb
Scale: 1250 lb/cm, 50 μsec/cm

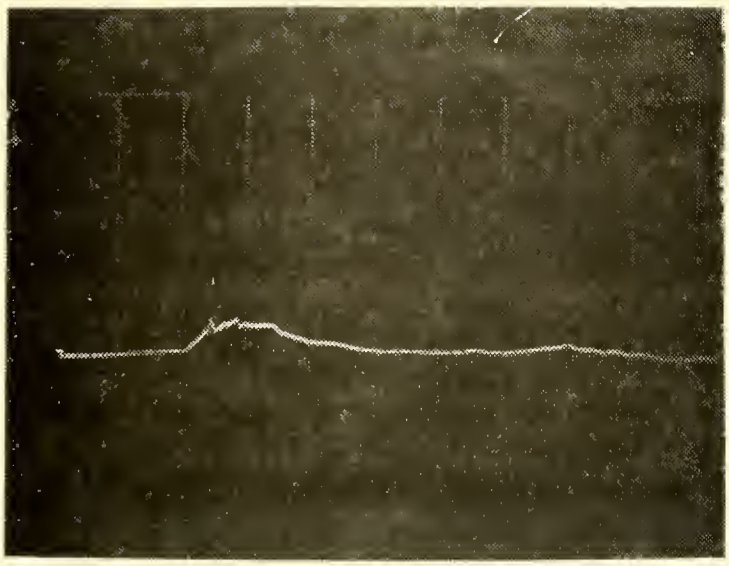

Radius = 6 in

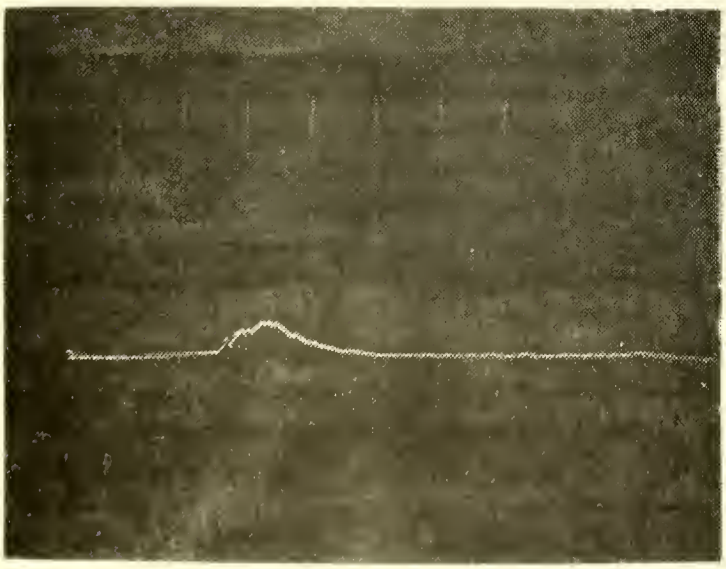

Radius = 7 in

Figure IV-3. Pressure vs. Time, E_o = 7,493 in-lb
Scale: 1250 lb/cm, 50 μsec/cm

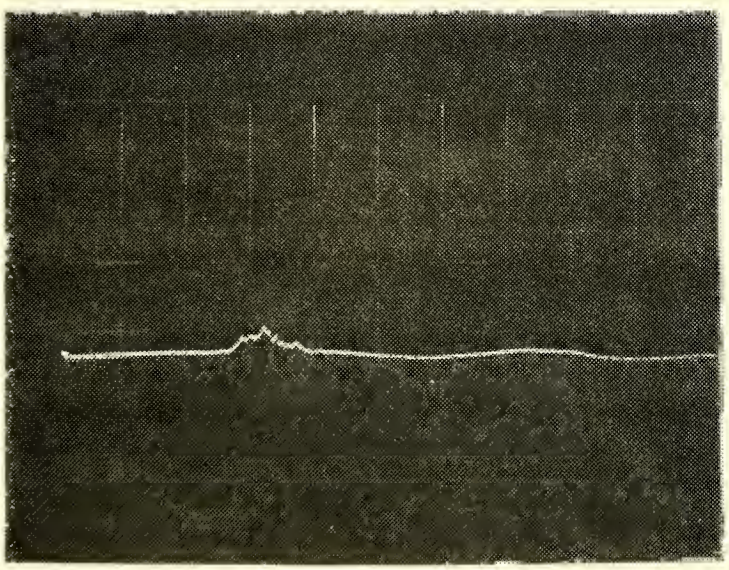

Radius = 8 in

Figure IV-4. Pressure vs. Time, E_o = 7,493 in-lb
Scale: 1250 lb/cm, 50 μsec/cm

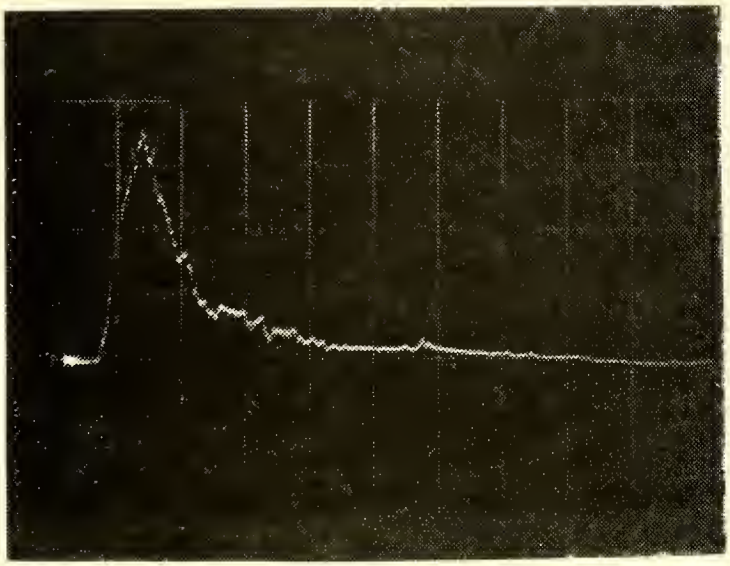

Radius = 2 in

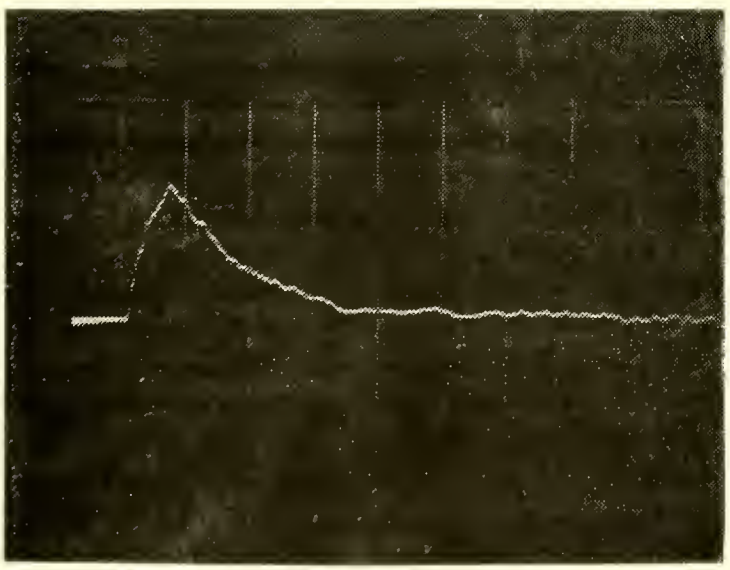

Radius = 3 in

Figure IV-5. Pressure vs. Time, E_o = 12,343 in-lb
Scale: 1250 lb/cm, 50 μsec/cm

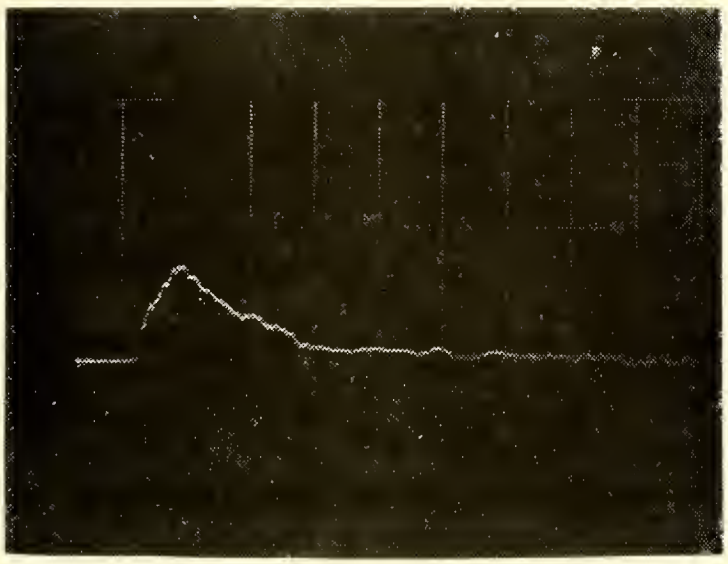

Radius = 4 in

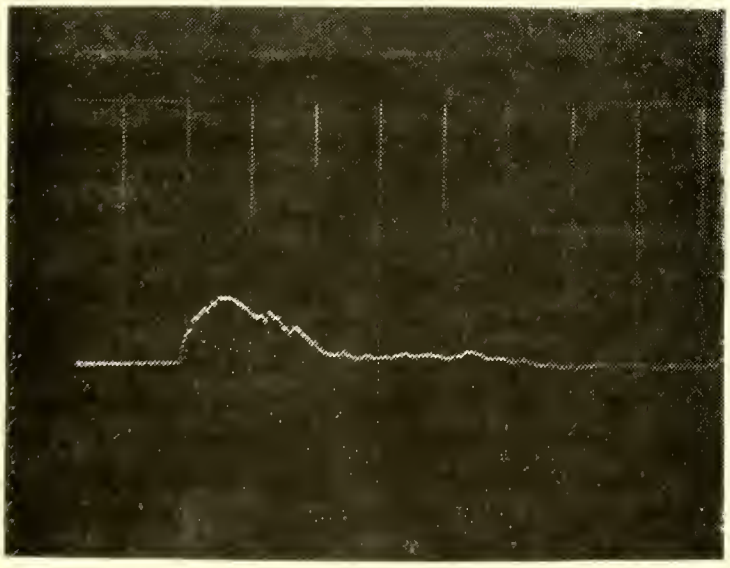

Radius = 5 in

Figure IV-6. Pressure vs. Time, E_o = 12,343 in-lb
Scale: 1250 lb/cm, 50 μsec/cm

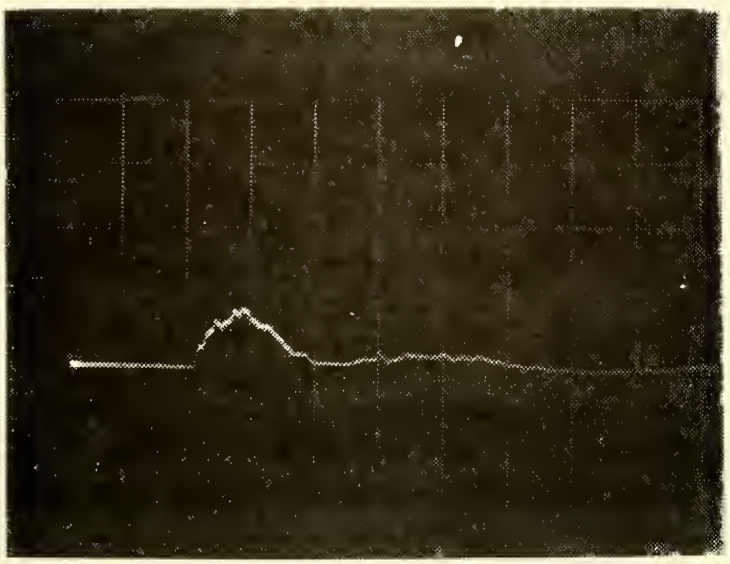

Radius = 6 in

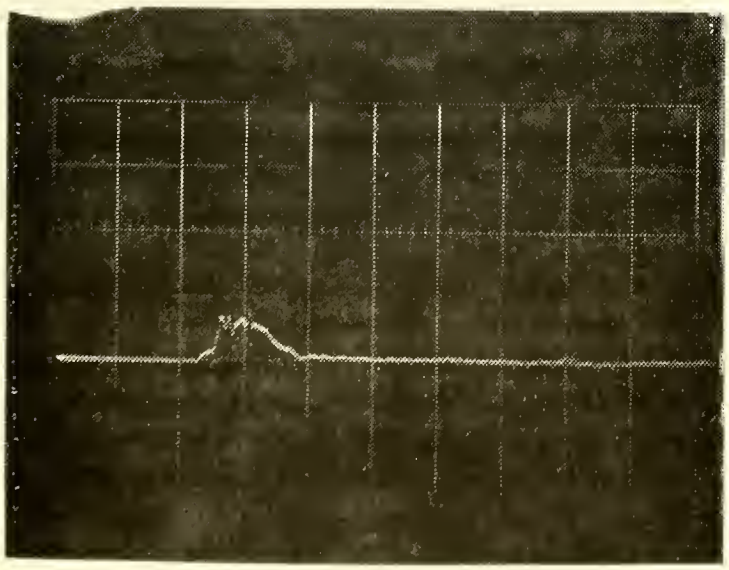

Radius = 7 in

Figure IV-7. Pressure vs. Time, E_o = 12,343 in-lb
Scale: 1250 lb/cm, 50 μsec/cm

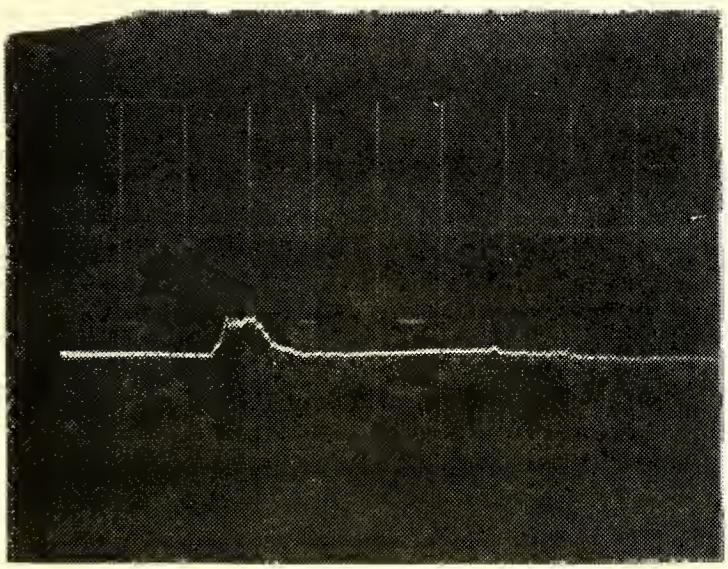

Radius = 8 in

Figure IV-8. Pressure vs. Time, E_o = 12,343 in-lb
Scale: 1250 lb/cm, 50 μsec/cm

point the pressure is several orders of magnitude greater than that calculated for the drag phase. Calculated pressures produced in the drag phase have durations of several hundreds of microseconds and are a function of the energy dissipation distribution as the bullet traverses the fluid. The time scales for the two phases are very different; therefore, the contribution each phase makes to the total pressure pulse may be assumed to be created independently of the other.

Theoretical pressure curves for these two phases, obtained from computer programs based on the Yurkovich and Lundstrom models, are compared with experimental results in Figures IV-9 through IV-14.

The theoretical shock phase pressure was computed using the theory of Yurkovich assuming a 10% loss of energy by the projectile during the shock phase of tank penetration. This energy loss was based on bullet velocity decay data obtained by Kappel for similar projectiles. A velocity decay of 5% was found to occur within the first 0.6 inch of fluid penetration. Both impact energy level data indicated similar energy losses on the order of 10% of the impact energy, the higher energy level percentage being only slightly greater. Accurate bullet velocity data were not available at shorter distances from the tank wall. Based on the data available, however, it was felt that the 10% figure used was a conservative estimate for calculation of the shock phase pressure pulse.

The Yurkovich model only predicts shock position and magnitude assuming the shock is strong. It was predicted that the shock front became acoustic at 1.32 inches from the impact point for the 7,493 in-lb energy level and at 1.55 inches for the 12,323 in-lb energy level. Acoustic theory was used to extend the Yurkovich model to larger radii. Cole [Ref. 8] has shown that the pressure of a spherical sonic wave decays inversely with the distance traveled and this relationship was used to calculate pressure decay. The wave front position was calculated assuming the wave front velocity was sonic (4900 feet per second in water).

The resulting shock phase pressure pulses have an abrupt, high peak pressure followed by a very rapid pressure decay that occurs in a few microseconds. A comparison of the two energy levels at equivalent radii provides an indication as to the effect of differing input energies. Peak pressure differences of almost 1000 lbs occur at the two-inch distance, with the differential decreasing with an increase in radius.

Figures IV-9, IV-11, IV-12 and IV-14 show that the maximum predicted duration of the shock phase is approximately 25 microseconds at eight inches and that the duration decreases to eight microseconds at a distance of two inches. The transducer and amplifier system used had a rise time of five to six microseconds; therefore, the peak pressures of the shock phase could not be measured. However, it was expected that the shock phase pulse length was long enough,

particularly at the larger distances, for the equipment to measure the decay of the shock induced pressures. Interaction of the drag and shock phase pressure pulses, however, precluded any direct observation of pressures created by the shock phase. Any future work to determine the shock phase pressure demands development of transducers with rise times on the order of hundreds of nanoseconds if the entire pulse is to be recorded.

It was predicted that pressures on the order of 1000 psi with a duration of 25 microseconds remain even at 8 inches from the impact point. In this case the pressures created by the shock phase at large distances may be of a sufficient magnitude and duration to cause significant damage to fuel cell components assuming the fuel cell is large enough so that the shock phase pressure pulse has not reflected from other walls.

Drag phase pressure pulses, obtained from the Lundstrom model, have lower peak pressures than those predicted for the shock phase. Pressure decay with time is slower by an order of magnitude than that expected for the shock phase and the predicted pressure durations are well over 100 microseconds. Predicted decreases of drag phase pressure with distance from the impact point are also less rapid than those predicted for the shock phase.

Drag phase pressures are produced as a result of projectile energy dissipation as the projectile traverses a fluid filled cell. The magnitude of the pressure produced

is a function of the rate of energy dissipation of the bullet. Peak pressures are lower than those created in the shock phase, particularly near the initial projectile impact point.

To calculate the drag phase pressures the bullet drag characteristics were computed from bullet position vs. time, shadowgraph work done by Kappel. An analysis of velocity decay suggested by Lundstrom was utilized as a basis for calculating the drag characteristics. The equation of motion was used

$$D = - m \frac{dV}{dt} = \frac{1}{2} \rho_f V^2 C_D A \qquad \text{IV-1}$$

Assuming constant drag coefficient, projectile mass, and projectile area it was possible to rearrange equation IV-1 and integrate, which yields:

$$\frac{V}{V_o} = e^{-(B)x} \qquad \text{IV-2}$$

where

$$B = \frac{\rho_f C_D A}{2m} \qquad \text{IV-3}$$

is the projectile velocity decay factor and V_o is the impact velocity.

Rearrangement and integration from initial conditions of x=0 at t=0 yields the following expression for projectile position as a function of time:

$$x = \frac{1}{B} \ln(BV_o t + 1) \qquad \text{IV-4}$$

If the fluid density and projectile mass are assumed constant then the bullet equivalent flat plate area

$$f = C_D A$$

may be determined by calculating the value of the constant B that best fits the data. In this way the rate of energy dissipation may be calculated.

Comparison of the analytical and experimental pressure traces for the drag phase shows that Lundstrom's analysis underestimates the peak pressures obtained in this particular situation. However, this program has achieved accurate results with 12.7 mm projectiles impacting larger tanks. The size of the drag phase cavity, compared with the dimensions of the tank used in this experiment, was one of the main causes of pressures higher than predicted. The close proximity of the walls to the cavity formed by the projectile probably had several effects. The computer program accurately predicts reflected pressures but only so long as wall reflections have not reached the cavity. Reflections off the cavity and their effect on pressure are not calculated. Wall restraining effects on cavity growth are also not estimated and contribute to the disparity in pressure values. The small tank used would make the pressure contributions of these effects more pronounced.

Figure IV-15 is a plot of the experimental peak pressure vs. distance from the impact point compared with the peak pressures obtained from the Lundstrom model. Experimental

peak pressure decay is approximately inversely proportional to the distance from the impact point. Lundstrom's theory does not predict this result. The pressure decay for the experimental data is similar to that experienced by an acoustic disturbance centered at the impact point.

Neither the Yurkovich nor the Lundstrom analysis appears to predict peak pressure or wave shape accurately enough for detailed design of ram-proof fuel cells. Considering the complexity of the hydraulic ram phenomenon and the simplicity of the two models, they are useful, however, in predicting peak pressures that are of the right order of magnitude. Tank configuration and size relative to the cavity size appear to have a sizable effects on the pressure developed by hydraulic ram phenomena.

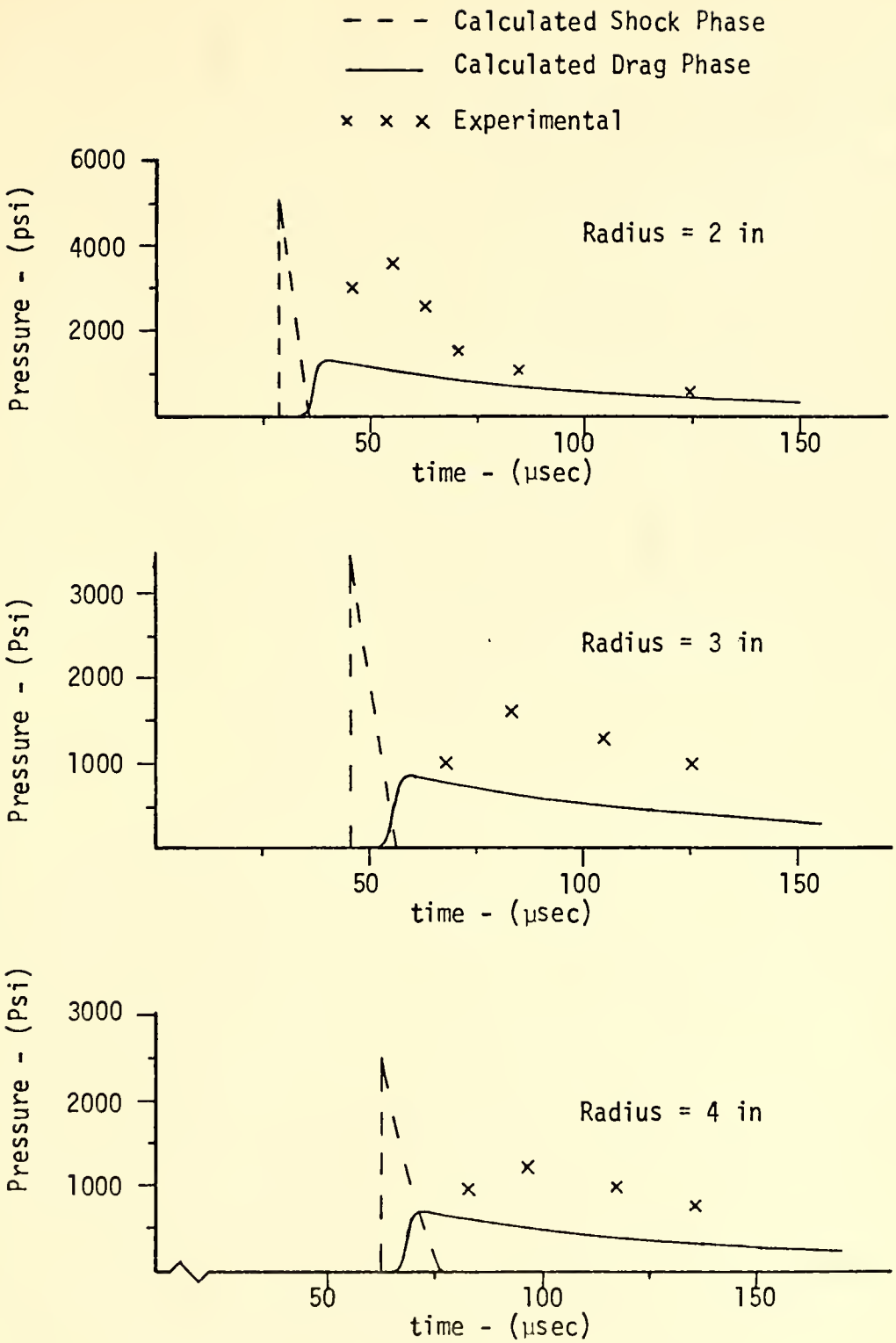

Figure IV-9. Pressure Comparison, E_o = 7,493 in-lb

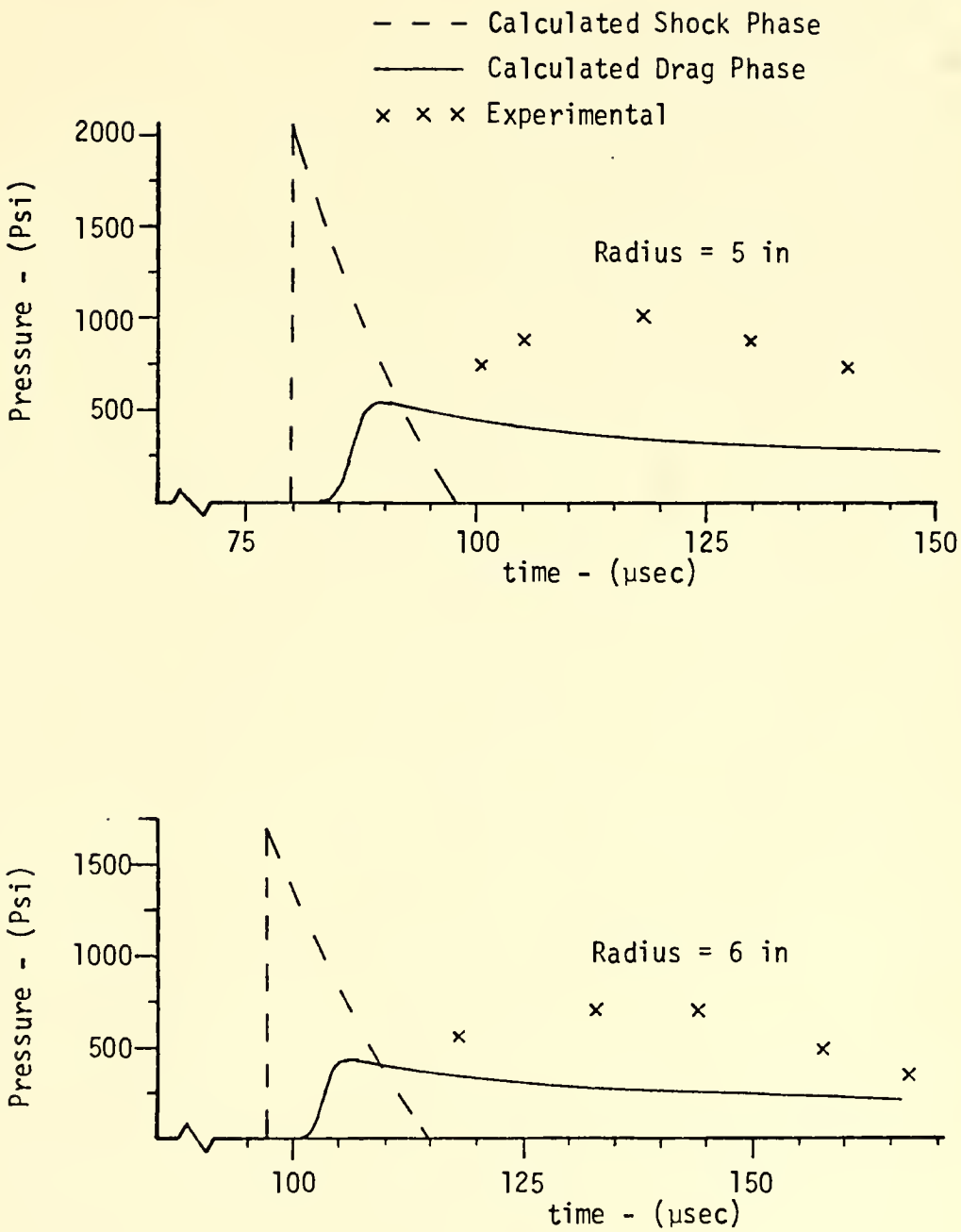

Figure IV-10. Pressure Comparison, E_o = 7,493 in-lb

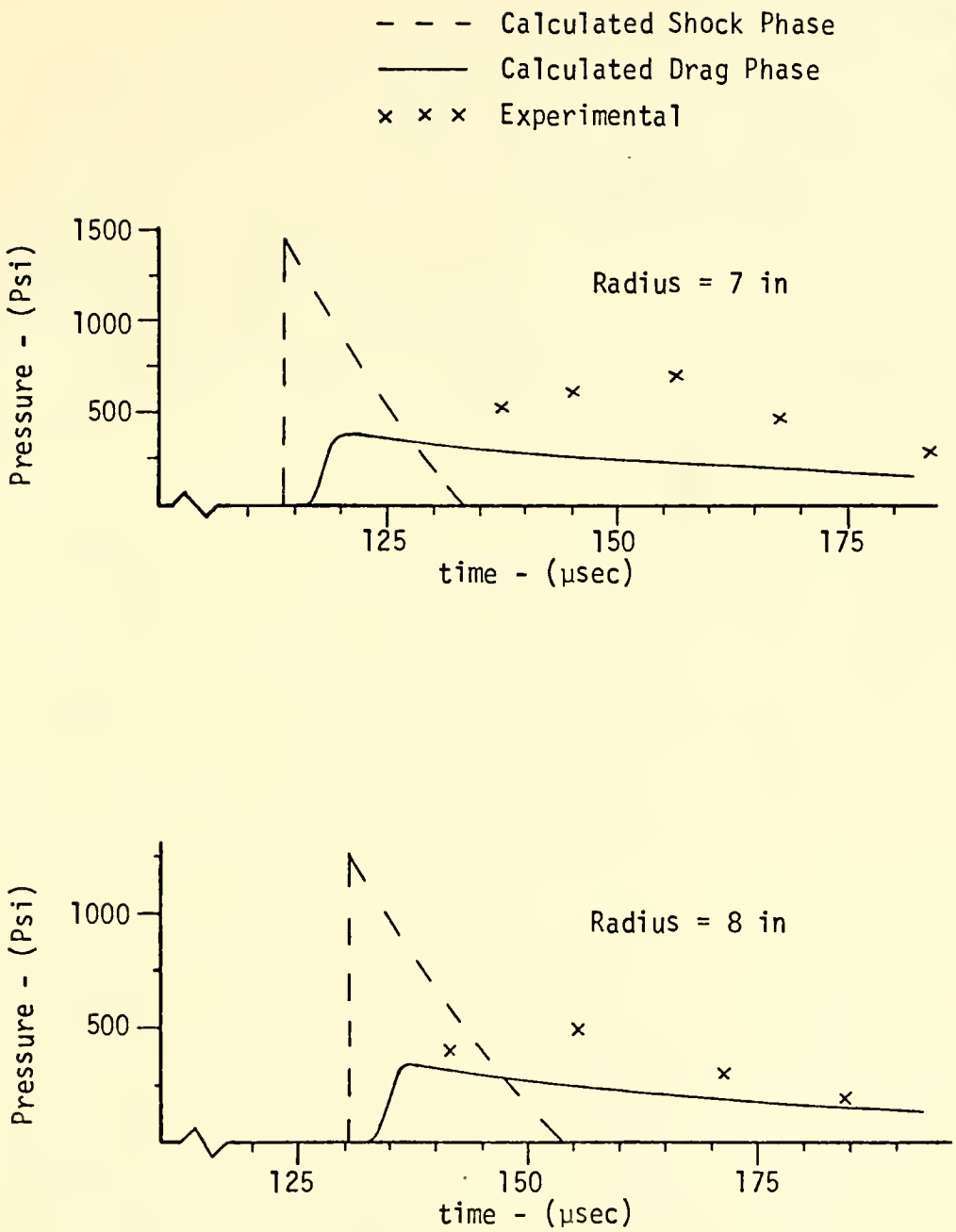

Figure IV-11. Pressure Comparison, E_o = 7,493 in-lb

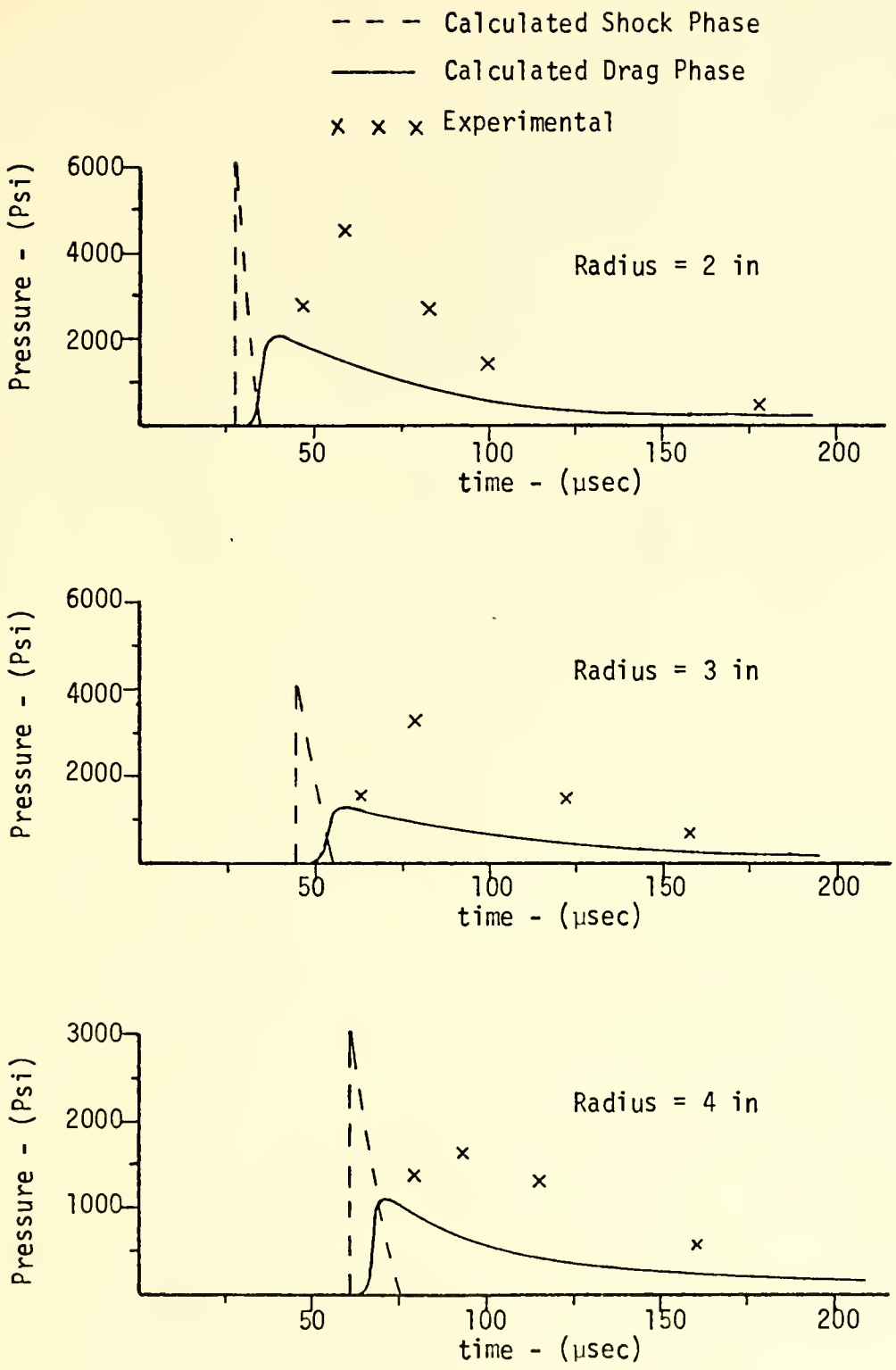

Figure IV-12. Pressure Comparison, E_o = 12,323 in-lb

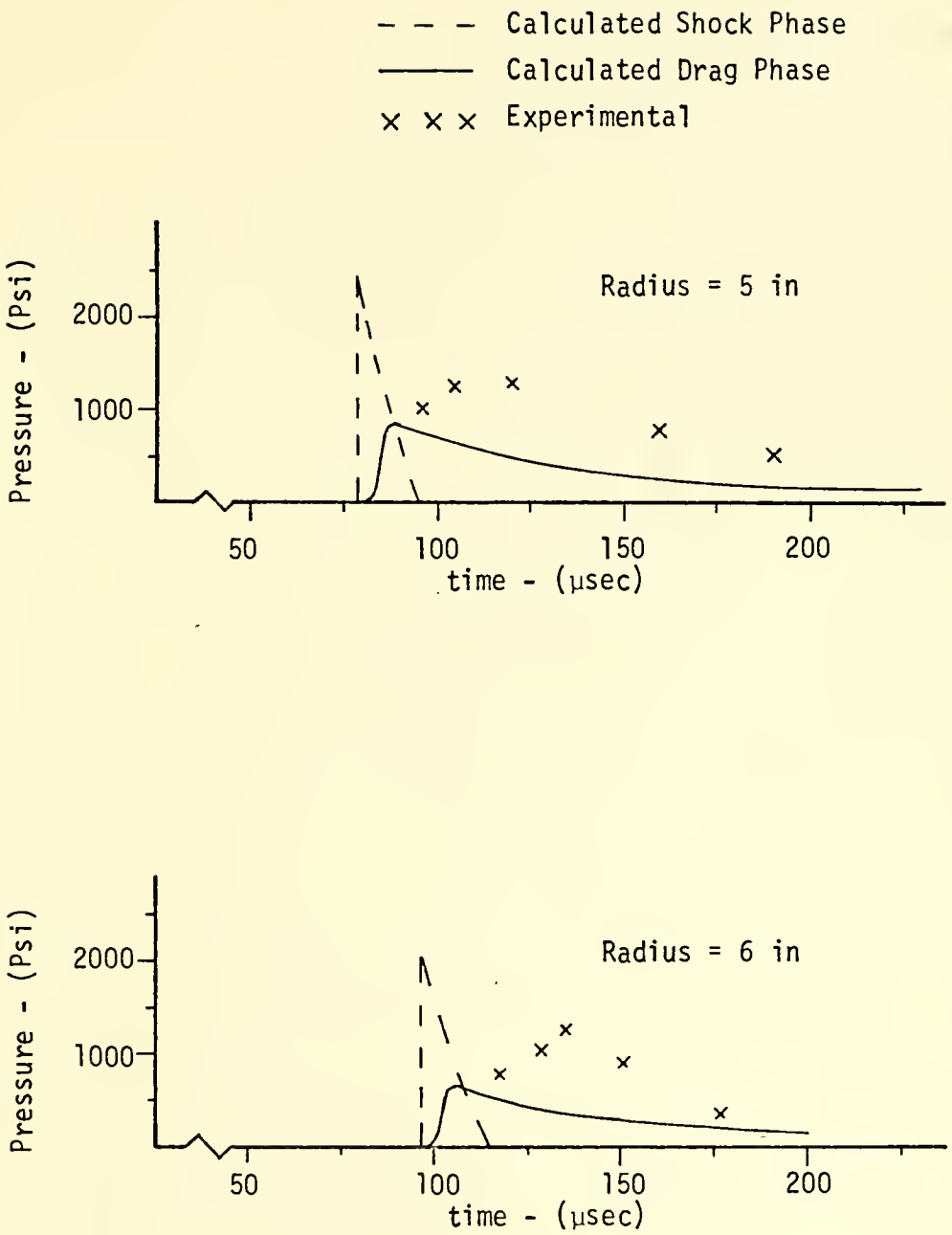

Figure IV-13. Pressure Comparison, E_o = 12,323 in-lb

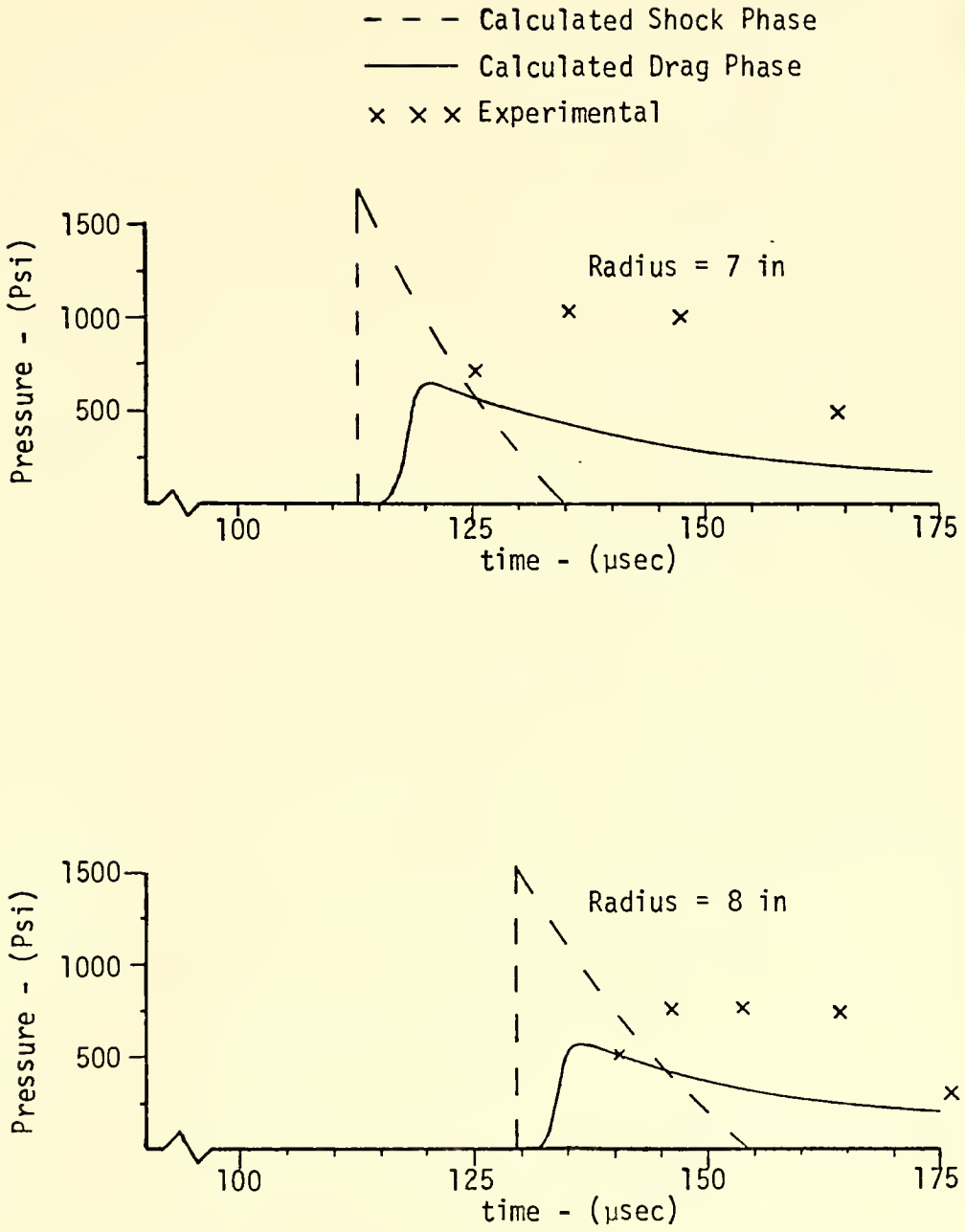

Figure IV-14. Pressure Comparison, E_o = 12,323 in-lb

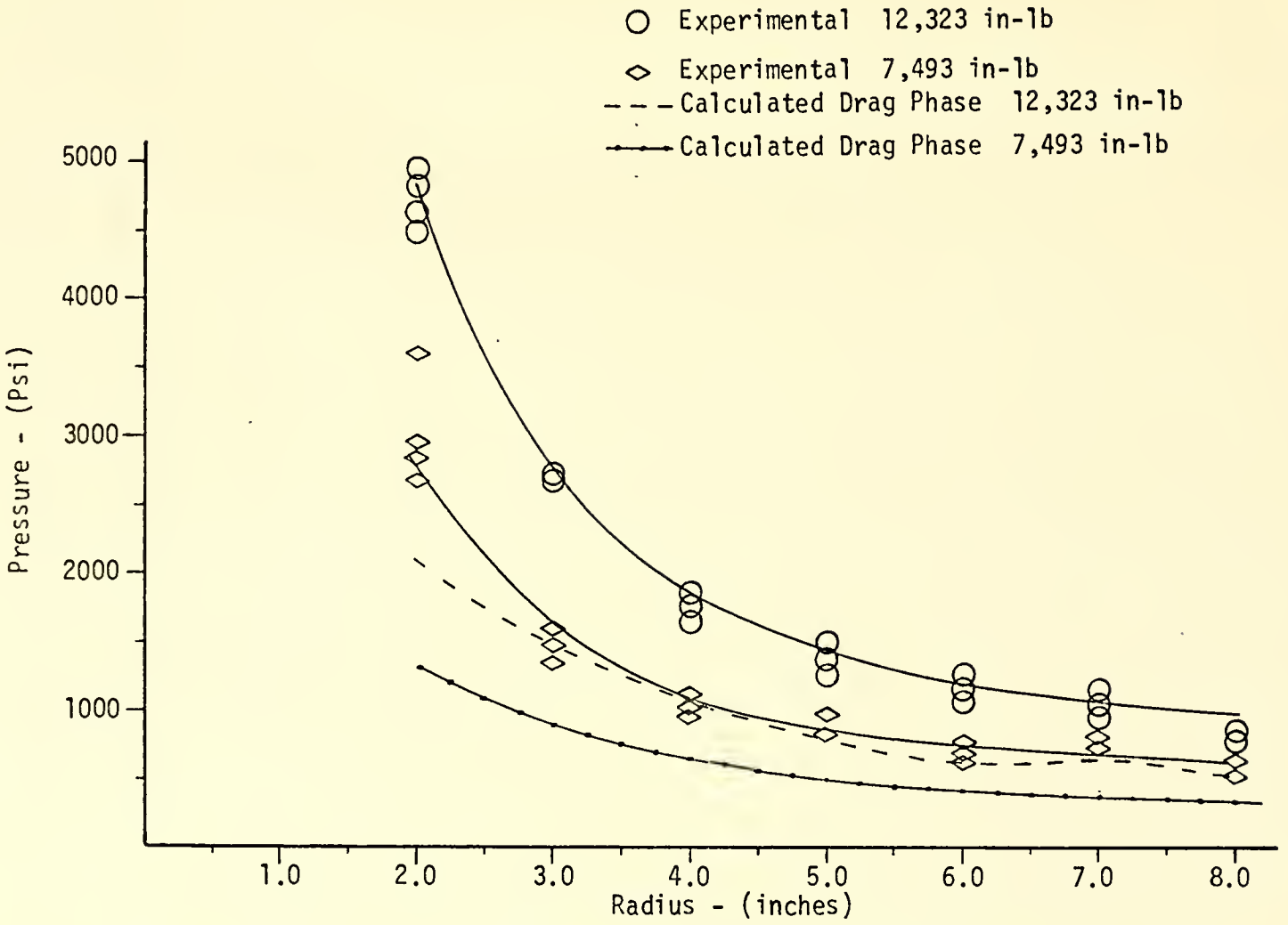

Figure IV-15. Peak Pressure vs. Radius for Two Energy Levels

V. RECOMMENDATIONS

The following recommendations are offered as an aid for further study of hydraulic ram phenomena.

1. Measurement of the shock phase pressure requires development of faster response time transducers. Response times as fast as hundreds of nanoseconds are required for accurate measurement of the shock pulse. It is recommended that transducers with these response characteristics be developed and used in any future investigation of the shock phase pressure field. Until this has been accomplished the damage contribution of the shock phase of hydraulic ram cannot be estimated accurately.

2. The Lundstrom model should be improved to consider more realistic wall pressure reflections so that wall pressure loadings may be predicted. A systematic study should also be made to determine the effects of the tank wall on cavity size and the resulting theoretical source distribution. This should improve the correlation of these experimental results with the Lundstrom model.

3. Fluid pressure measurements at the wall surface should be employed in a structural analysis to obtain theoretical wall strains using the SATANS [Ref. 9] structural computer code. These results should be compared with actual strains so that tank wall motion and damage can be estimated.

LIST OF REFERENCES

1. Naval Weapons Center Technical Publication, 5227, Fluid Dynamic Analysis of Hydraulic Ram, by E.A. Lundstrom, July 1971.

2. McDonnel Aircraft Engineering Methods Authorization, F65-76-555, Hydraulic Ram: A Fuel Tank Vulnerability Study, by R.N. Yurkovich, September 1969.

3. Douglas Aircraft Company Contract N00019-69-G-0181, Fuel Tank Vulnerability Reduction, by H.F. Winchester, J.F. Denlinger, G.A. Vickers, W.R. Dunbar, and L.D. Christensen, April 1970

4. NASA Technical Note, NASA TN D-3143, Investigation of Characteristics of Pressure Waves Generated in Water Filled Tanks Impacted by High Velocity Projectiles, by F.S. Stepka, C.R. Morse, and R.P. Dengler, December 1965.

5. McMillen, J. Howard, "Shock Wave Pressures in Water Produced by Impact of Small Spheres," Physical Review, v. 68, p. 198-208, 1 November 1945.

6. Power, H.L., "FY 74 Experimental Hydraulic Ram Studies," NPS-57Ph74081, August 1974.

7. Kappel, L.S., "Hydraulic Ram Shock Phase Effects on Fuel Cell Survivability," MSAE Thesis, Naval Postgraduate School, Monterey, California, March 1974.

8. Cole, R.H., Underwater Explosions, Princeton University Press, 1945.

9. Ball, R.E., "A Program for the Nonlinear Static and Dynamic Analysis of Arbitrarily Loaded Shells of Revolution," Computers and Structures, v. 2, p. 141-162, 1972.

INITIAL DISTRIBUTION LIST

		No. Copies
1.	Defense Documentation Center Cameron Station Alexandria, Virginia 22314	2
2.	Library, Code 0212 Naval Postgraduate School Monterey, California 93940	2
3.	Chairman, Department of Aeronautics, Code 57 Naval Postgraduate School Monterey, California 93940	1
4.	Professor H. L. Power, Jr., Code 57Ph Department of Aeronautics Naval Postgraduate School Monterey, California 93940	6
5.	Professor R. E. Ball, Code 57Ba Department of Aeronautics Naval Postgraduate School Monterey, California 93940	1
6.	Captain James McNerney DDR & E Pentagon Department of Defense Washington, D.C. 20301	1
7.	CDR Merlin L. Johnson Naval Air Systems Command Washington, D.C. 20360	1
8.	CDR D. Hicks Naval Air Systems Command Washington, D.C. 20360	1
9.	Mr. Andy Holton AFDL/PTS Wright Patterson AFB Ohio 45433	1
10.	LT. Clifford M. Holm 423 Oswego Street Aurora, Colorado 80010	2
11.	Mr. Wallace K. Fung, Code 5114 Naval Weapons Center China Lake, California 93555	2

Thesis
H6885 Holm
c.1
157034
Hydraulic ram
pressure measurements.